Pb, Cu, and Zn distributions at Humic Acid-Coated Metal-Oxide Surfaces

Yingge Wang[a], F. Marc Michel[a,b,+], Clement Levard[a,‡], Yongseong Choi[c], Peter J. Eng[d], Hagar Siebner[a], Baohua Gu[e], John R. Bargar[b], and Gordon E. Brown, Jr.[a,b,f,g,*]

[a]*Surface & Aqueous Geochemistry Group, Dept. of Geological & Environmental Sciences, Stanford University, Stanford, CA 94305-2115, USA*

[b]*Stanford Synchrotron Radiation Lightsource, SLAC National Accelerator Laboratory, MS 69, 2575 Sand Hill Road, Menlo Park, CA 94025, USA*

[c]*Advanced Photon Source, Argonne National Laboratory, 9700 South Cass Ave., Argonne, IL 60439, USA*

[d]*Consortium for Advanced Radiation Sources, University of Chicago, Chicago, IL 60637, USA*

[e]*Oak Ridge National Laboratory, Environmental Science Division, Oak Ridge, TN 3783, USA*

[f]*Dept. of Photon Science, SLAC National Accelerator Laboratory, 2575 Sand Hill Road, Menlo Park, CA 94025, USA*

[g]*Dept. of Chemical Engineering, Stanford University, Stanford, CA 94305, USA*

To be submitted to *Geochim. Cosmochim. Acta*

*Corresponding author address: Green Earth Science Bldg., 367 Panama St., Room 309, Stanford, CA 94305-2115. Tel.: +1 650-723-9168, fax: +1 650-729-2199

Email: gordon.brown@stanford.edu

[+]Present address: Dept. of Geosciences, Virginia Tech, Blacksburg, VA 24061, USA

[‡]CEREGE, Europôle Méditerranéen de l'Arbois, BP 80, 13545 Aix en Provence, Cedex 04, France

Abstract

Mineral surfaces are often coated by natural organic matter (NOM), which has a major influence on metal-ion sorption and sequestration because the abundance of binding sites in such coatings and the changes in local nanoscale environments they cause. The effects of NOM coatings on mineral surfaces are, however, still poorly understood at the molecular level due to the complexity of these systems. In this study, we applied long-period x-ray standing wave-florescence yield (LP-XSW-FY) spectroscopy to measure the partitioning of naturally present Cu(II), Zn(II), and Pb(II) between Elliott soil humic acid (ESHA) coatings and three model single-crystal metal-oxide substrates: α-Al_2O_3 (0001) and (1-102) and α-Fe_2O_3 (0001). The competitive sorption effects among these metal ions for binding sites in the ESHA coatings and on the metal-oxide surfaces were investigated as a function of reaction time, calcium content, and solution pH. Pb(II) ions present in the ESHA coatings were found to redistribute to reactive α-Al_2O_3 (1-102) and α-Fe_2O_3 (0001) surfaces after 3 hours of reaction (pH = 6.0, [Ca(II)] = 2 mM). Pb(II) partitioning onto these reactive metal-oxide surfaces increased with increasing reaction time. However, no change in the partitioning of Cu(II) and Zn(II) onto the α-Al_2O_3 (1-102) surfaces was observed with reaction time, suggesting that these ions strongly complexed with functional groups in the ESHA coatings. Similar results were obtained for Cu(II) and Zn(II) on the ESHA-coated α-Al_2O_3 (1-102) surfaces in the samples without the addition of calcium. However, the amounts of Pb(II) mobilized from the ESHA coatings onto the α-Al_2O_3 (1-102) surfaces with 2 mM calcium added increased slightly after 24 hours of reaction time possibly due to displacement of Pb(II) by Ca(II) from the binding sites of ESHA coatings. In contrast, Pb(II), Cu(II) and Zn(II) present in the ESHA coatings were found to be unreactive with the α-Al_2O_3 (0001) surface. The observed reactivities of the three ESHA-coated metal-oxide surfaces with respect to metal-ion sorption are consistent with the trend observed for the uncoated metal-oxide surfaces: α-Fe_2O_3(0001) > α-Al_2O_3(1-102) > α-Al_2O_3(0001). In addition, Pb(II) partitioning onto α-Al_2O_3 (1-102) surfaces increased with increasing pH from 4.0 to 9.0 as a result of the increasing negative surface charge. These results show that intrinsic properties (nature of binding sites, binding affinities, and surface charge) of the ESHA coatings and metal-oxide surfaces, as well as external parameters such as pH, are key factors governing the distribution and speciation of metal ions at complex NOM/mineral interfaces.

1. INTRODUCTION

NOM is ubiquitous in terrestrial and aqueous ecosystems, and humic substances are the predominant species of NOM in water, soil, and sediment environment (Leenheer et al., 1994; Aiken and Cotsaris, 1995; Benedetti et al., 1995; Gu et al., 1996a; Kinniburgh et al., 1999; Tipping, 2002; Koopal et al., 2005). The properties and concentrations of humic substances vary significantly with source because they are heterogeneous mixtures of biochemical degradation products from plant and animal residues (Aiken and Cotsaris, 1995; Tipping, 2002). For example, the concentration of humic substances in groundwater can vary from 1 to 70 mg/l (Thurman E.M., 1982; Herbert and Bertsch, 1995) in soil water as dissolved organic carbon (DOC), whereas the DOC concentration in surface waters can range from 0.5 to 100 mg/L with an average concentration of 5 mg/L, and the DOC concentration in oceans is found to be 1 mg/L in the surface and 0.5 mg/L at depth (Tipping, 2002). The soil content of humic substances can vary from less than 1% in some sandy soils to 100% in peats (Tipping, 2002). The effective concentration of humic substances (mass of humic matter per unit volume of soil water) can be found as high as 60 g/L in B horizons of forest soils, and 5 g/L in the typical marine sediment (Lofts et al., 2001; Tipping, 2002). Humic substances can be present in very high effective concentrations in soil and aquatic sediments, and thus potentially influence metal-ion distributions in natural environments (Tipping, 2002).

Humic substances are complex mixtures of organic macromolecules containing various reactive functional groups such as carboxylic (-COOH), phenolic (-OH), amino (-NHR, -NH_2), and thiol (-RS) (Tipping, 1993; Leenheer et al., 1994; Gu et al., 1996a; Gu et al., 1996b; Kinniburgh et al., 1999; Tipping, 2002; Koopal et al., 2005; Van Riemsdijk et al., 2006; Rey-Castro et al., 2009). Anionic functional groups (e.g., carboxylic) introduce negative charges and have a strong affinity for positively charged mineral surfaces, and thus often partially coat fine-grained minerals such as the common metal-(oxy)hydroxide minerals in soils (Neihof and Loeb, 1974; Davis, 1984; Ransom et al., 1997; Au et al., 1999; Mayer, 1999; Bonneville et al., 2012; Lalonde et al., 2012). Neihof and Loeb (1974) introduced the concept known as the "effective monolayer hypothesis", which postulates that most particles in marine environments are coated by thin films (effective monolayers) of organic matter. This hypothesis led to the notion that adsorption properties of marine particles are controlled by organic coatings (Balistrieri et al.,

1981; Davis, 1984), which was followed by the notion that most particles in soils and aquatic systems are coated by a thin organic film (Mayer, 1994; Au et al., 1999). However, Ransom et al. (1997) found that most organic matter and microbial coatings in continental margin sediments are patchy in distribution and discontinuously associated with clay minerals, thus refuting the effective monolayer hypothesis. In a subsequent study, Mayer (1999) concluded that less than 15% of particle surfaces are covered by organic matter in marine aluminosilicate sediments with low to moderate loadings of organic matter (< 3 mg organic carbon/m^2). Mayer and Xing (2001) further suggested that organic carbon content in B and C horizons of acidic soil samples is at the monolayer equivalent level (~ 1 mg organic carbon/m^2), whereas the organic carbon content in surfacial A and O horizons exceeds that level. Nonetheless, soil organic matter is often closely associated with mineral surfaces. Lalonde et al. (2012) reported that 21.5±8.6 percent of organic carbon is directly bound to reactive iron-oxide phases in sediment samples from a wide range of deposition environments, suggesting that reactive iron-oxide phases serve as an "extremely efficient rusty sink" for organic carbon.

The presence of such organic coatings on mineral surfaces could potentially induce steric and electrostatic changes that modify the physicochemical properties of colloidal mineral particles such as surface charge and colloidal stability, and substantially alter the sorptive capacity of metal-(oxy)hydroxide minerals (e.g., Davis, 1984; Tipping, 2002; Gu et al., 1996b). In addition, various reactive functional groups present in humic substances are known to form strong complexes with metal contaminants such as Cu, Zn, Pb, and Hg, making them potentially important environmental sorbents and a major influence on the fate and transport of metal contaminants in environmental systems (Benedetti et al., 1995; Kinniburgh et al., 1999; Tipping, 2002). A recent study of the speciation of airborne Pb using x-ray adsorption spectroscopy demonstrated that the major species of Pb in air is primarily Pb-humate, suggesting that the Pb is from soils (Pingitore et al., 2009). Understanding how metal ions interact with NOM and minerals in the soil is essential for evaluating the transport and fate of metal ions in our environment.

There have been extensive studies of the interaction of humic substances with aqueous metal ions and mineral surfaces in contact with aqueous solutions (Benedetti et al., 1995; Kinniburgh et al., 1999; Wightman and Fein, 2001; Tipping, 2002; Tipping et al., 2002; Tombacz et al., 2004;). However, the potential effects of organic coatings on mineral surface reactivity and their

influence on metal-ion sorption and cycling are largely unverified experimentally due to the complexity of the systems and the lack of appropriate analytical tools. As a result, qualitative and quantitative information about metal-ion partitioning between mineral surfaces and organic coatings is required for better understanding of metal cycling under realistic environmental conditions.

The availability of high intensity synchrotron light sources has resulted in new analytical methods that can provide quantitative information on the partitioning of metal ions between mineral surfaces and NOM or microbial biofilm coatings. Batterman and Golovchenko and co-workers introduced x-ray standing wave spectroscopy on surfaces in several classic papers (Batterman, 1964; Batterman and Cole, 1964; Golovchenko et al., 1974; Cowan et al., 1980) and pointed out the utility of both long-period and short-period (or Bragg) x-ray standing wave florescent yield spectroscopy for probing the distribution of metal ions at buried interfaces. Subsequently, the long-period x-ray standing wave fluorescent yield (LP-XSW-FY) method has been used to probe the vertical distribution of atoms at a number of different types of interfaces, including electrochemical interfaces (Bedzyk et al., 1986; Abruna et al., 1989); biological membranes (Bedzyk et al., 1988; Bedzyk et al., 1990; Wang et al., 1991; Wang et al., 1992), organic thin films (Bedzyk, 1992), and mineral surfaces coated with microbial biofilms or thin organic films (Templeton et al., 2001; Templeton et al., 2003; Yoon et al., 2005; Levard et al., 2011). Two references provide excellent reviews of these various applications of LP-XSW-FY spectroscopy through 2006 (Bedzyk and Cheng, 2002; Trainor et al., 2006)

The LP-XSW-FY technique requires a reflecting surface and generates a well-defined intensity field from the superposition of the incident and reflected x-ray beams on the reflective surface in grazing incidence mode under total reflectance conditions (Bedzyk and Cheng, 2002; Trainor et al., 2006). The generated standing wave can excite x-ray fluorescence from the elements present within thin films, and the resulting x-ray fluorescence emission can be detected using an energy dispersive x-ray detector, from which the vertical distribution of the elements present can be obtained (Bedzyk and Cheng, 2002; Trainor et al., 2006). The LP-XSW-FY technique provides a spatially localized periodic probe with a sub-nanometer scale XSW period that is particularly well suited for studying trace element distributions within thin films or layered samples including microbial biofilm- and organic film-coated mineral surfaces (Bedzyk and Cheng, 2002; Trainor et al., 2006). In addition, the energy of incident x-rays can be tuned to

simultaneously excite multiple elements present in a thin-film coating on a mineral surface, which provides a new capability for probing the interactions of various elements present in trace concentrations, including competitive effects among multiple metal ions for binding sites within the thin films and on the mineral surfaces.

Templeton and co-workers (Templeton et al., 2001) first applied the LP-XSW-FY approach to investigate *in situ* Pb(II) distributions on monolayer biofilm (*Burkholderia cepacia*) coated metal-oxide surfaces and found that the biofilm coatings did not block the reactive sites of the mineral surfaces. In a related study, we applied LP-XSW-FY spectroscopy to probe *in situ* Pb(II) and Zn(II) distributions on multilayer biofilm (*S. oneidensis* MR-1)-coated metal-oxide surfaces and found that even thick reactive biofilms do not change the intrinsic reactivity of the underlying mineral surfaces (Wang et al., submitted-I). We have also used the LP-XSW-FY method (Yoon et al., 2005) to probe Pb(II) and As(V) speciation and distribution at polyacrylic acid (PAA)-coated single-crystal α-Al_2O_3 and α-Fe_2O_3 substrates at pH 4.5, and found that the partitioning of these ions depends on the properties of the PAA film (i.e. carboxylate content) as well as on the intrinsic reactivities of the metal-oxide substrates. In the present study we investigated the partitioning of metal ions at natural organic matter (NOM)/metal-oxide interfaces using a model soil humic acid.

Reaction kinetics in metal-NOM-mineral systems is another important component of the present study. In the past, modeling/predicting trace metal distributions and speciation was mainly based on data obtained under equilibrium conditions (Buffle et al., 2007; Louis et al., 2009). However, fluctuating physicochemical conditions in natural systems such as rivers, lakes, estuaries, and oceans can lead to systems far from equilibrium (Tipping, 2002; Buffle et al., 2007; Louis et al., 2009). Many past experimental studies of NOM-metal interactions have not taken reaction kinetics into account or they assume fast kinetics so that the system is under equilibrium as a simplification (Tipping, 2002; Van Riemsdijk et al., 2006; Louis et al., 2009). Predictions of metal speciation in natural systems based on such assumptions should be viewed with caution (Hering and Morel, 1988a; Hering and Morel, 1988b; Tipping, 2002; Buffle et al., 2007; Louis et al., 2009). If reactions are slow, the application of speciation models to natural aquatic systems may result in overestimation of metal toxicity (Hering and Morel, 1988b;Tipping, 2002; Louis et al., 2009). To date, only a few studies have characterized the kinetics of trace metal complexation with simple ligands such as EDTA and/or extracted humic

substances (Hering and Morel, 1988b; Tipping, 2002; Louis et al., 2009). Hering and Morel (1989) showed that the kinetics of trace metal complexation can be considerably lowered in marine environments due to the competitive effect with calcium and magnesium cations (Hering and Morel, 1989). Slow dissociation rates of aqueous Ca–Mg NOM-complexes and competition with other trace elements are the key factors controlling reaction kinetics in such systems (Hering and Morel, 1988b; Hering and Morel, 1989).

In the present study, we chose Elliott Soil Humic Acid (ESHA) as a coating on Al-oxide and Fe-oxide substrates. ESHA is a model soil humic acid that has known physicochemical properties (IHSS). An ESHA concentration of 10 g/L was chosen as representative of the humic acid concentration in soil waters. At this concentration the ESHA coatings contain substantial amounts of metal ions (~0.0002-0.05%) that were originally present in the native form of ESHA, which allowed us to investigate the partitioning of these trace metal ions between the metal-oxide surfaces and the ESHA coatings as a function of time, without introduction of any additional metals to the system. Solution chemistry conditions, including pH and calcium content, were varied to study their effects on trace metal-ion partitioning. Oriented, single-crystal surfaces of α-Al_2O_3 (0001) and (1-102) and α-Fe_2O_3 (0001) were chosen as model metal-oxide surfaces. The use of different crystallographic orientations of single-crystal Fe- and Al-oxides provides information on intrinsic differences in chemical reactivity of different crystallographic surfaces of these common metal oxides (Eng et al., 2000; Trainor et al., 2002; Trainor et al., 2004; Tanwar et al., 2007).

2. MATERIALS AND METHODS

2.1. Crystal preparation

The single-crystal alumina surfaces were highly polished α-Al_2O_3(0001) and α-Al_2O_3(1-102) purchased from Saint-Gobain Crystals & Detectors Co. The single-crystal α-Fe_2O_3(0001) surfaces were prepared from natural specular hematite from Bahia, Brazil. The hematite crystals were cut into approximately 1 cm^2 wafers of ~2 mm thickness and polished parallel to (0001) natural growth surface using a chemical-mechanical polishing (CMP) procedure that produced surfaces of sufficient quality for x-ray reflectivity and LP-XSW-FY measurements in previous

218 studies (Eng et al., 2000; Trainor et al., 2002; Trainor et al., 2004; Yoon et al., 2005; Tanwar et
219 al., 2007). The r.m.s. surface roughness is consistently less than 5 Å for these wafers determined
220 by atomic force microscopy (Veeco Multimode Scanning probe microscope). The polished
221 crystal substrates were then carefully cleaned with acetone, then washed in $10^{-3.5}$ M sodium
222 hydroxide for 20 minutes, and subsequently washed in 10^{-2} M nitric acid for an hour. Each
223 chemical washing step was followed by extensive rinses with MilliQ water. The commercial α-
224 Al_2O_3 crystals (1-inch square α-Al_2O_3 (1-102) wafers and 2-inch diameter α-Al_2O_3 (0001)
225 wafers) were also cleaned as described above and then baked at 350°C for 4 hrs to minimize
226 excess carbon on the surfaces. This cleaning procedure was repeated as necessary until impurity
227 metals on the surfaces were undetectable (<0.1%) and the organic (adventitious) carbon on the
228 surfaces was less than ~10% as determined by x-ray photoelectron spectroscopy (XPS) (Surface
229 Science S-Probe, monochromatic Al Kα radiation).
230
231 **2.2. Deposition of NOM coatings**
232
233 Elliot Soil Humic Acid (ESHA) was purchased from the International Humic Substance
234 Society (IHSS, 1S102H) and used without further purification. ESHA stock solutions of 10 g/L
235 were prepared by dissolving the ESHA powder into N_2 sparged 0.01M $NaNO_3$ solution. The
236 solution pH was adjusted to 6.0 and equilibrated overnight using an end-over-end rotator; any
237 deviation from pH 6.0 was adjusted by adding small volumes of 0.01N NaOH or 0.01N HNO_3
238 solution. Depending on experimental conditions, 2 mM $Ca(NO_3)_2$ was added to some of the
239 ESHA solutions to test the effect of calcium on metal-ion partitioning. The ESHA solutions were
240 then filtered using 0.2 μm glass filters. All ESHA solutions were kept in the dark at all times to
241 prevent any photo degradation. Each clean metal-oxide substrate was placed inside a Petri dish.
242 A 200-μl aliquot of ESHA solution was then pipetted onto each crystal surface and equilibrated
243 for the desired reaction time ranging from 3 hours to 7 days. A wet Kimwipe^{TM} was kept inside
244 the closed Petri dish to reduce evaporation. After reaction, the samples were taken to a spin
245 coater (Headway Research, Inc., EC101DT spinner), and the reacted ESHA solutions were spin-
246 coated dry onto the metal-oxide surfaces at 1300 rpm for 40 seconds.
247 The trace metal contents of ESHA solutions were measured by inductively coupled plasma
248 atomic emission spectroscopy (ICP-AES). Because of the interference of the high organic carbon

content with the metal analyses, ESHA solutions were diluted from 10 g/L to 0.5 g/L to obtain acceptable data from ICP-AES. C K-edge near edge x-ray absorption fine structure (NEXAFS) spectroscopy data were collected at the scanning transmission x-ray microscopy (STXM) end station of beam line 11.0.2.2 at the Advanced Light Source (Lawrence Berkeley National Laboratory). 2-µl droplets of freshly prepared 0.1g/L ESHA solutions were placed on 100 nm-thick Si_3N_4 membranes, and allowed to air dry in a clean hood. Elemental distribution maps were obtained by subtracting images taken at energies below the absorption edge of the element of interest from images taken at energy slightly above the absorption edge. Image stacks were collected by scanning a predetermined area (~ 5-10 µm) of the sample in the x-y directions, at an energy increment of 0.1 eV over the energy range of interest (280-310 eV for the C K-edge). Energy calibration was done initially using the peak at 294.96 eV of gaseous CO_2 for the C K-edge. Normalization and background correction of the C K-edge NEXAFS spectra were performed by dividing each spectrum by a second spectrum from a C-free location on the same sample. The aXis2000 software package was used for image and spectral processing (Hitchcock, 2000). ICP-AES and STXM analysis were also performed for Suwannee River Humic Acid (SRHA) and Suwannee River Fulvic Acid (SRFA) using the same procedure for comparison.

2.3. LP-XSW-FY measurements and data analysis

LP-XSW-FY measurements were performed at the GSECARS sector on undulator beamline 13-ID-C at the Advanced Photon Source (APS) using a general-purpose Kappa diffractometer. X-rays were monochromatized using a liquid N_2-cooled Si(111) monochromator and were focused using Rh-coated double-focusing mirrors. The x-ray beam was collimated to 1.0 mm vertical and 20 µm horizontal. Samples were mounted in a Teflon™ sample cell covered with a polypropylene film, and the space over the sample was purged by dry helium gas during the experiments. The x-ray incidence angle was scanned between 0.0 and 0.5° in 0.002° steps for the x-ray reflectivity measurements while the incident (I_0) and reflected (I_1) x-rays were monitored through N_2-filled gas ionization chambers. The fluorescence yield of various trace metal ions was collected at 14 keV incident energy. Fluorescence spectra were acquired using a 4-element silicon drift detector (SII NanoTechnology, Vortex-ME4) coupled to digital x-ray processor electronics (X-ray Instrumentation Associates, xMAP). The detector array was located in the

horizontal plane and 90° to the incident beam in order to suppress the charge scattering background from the sample. Each of the four detector elements was fit with a collimator so that it could only detect the x-ray foot print at the center of the sample and thus block scatter and fluorescence x-rays from background being collected by the detector. The fluorescence yield spectrum from each of the four detector elements was averaged and corrected for deadtime. The total area of each fluorescence peak was fit using a Gaussian line shape on a linear background. Repetitive scans of LP-XSW-FY and reflectivity profiles with the x-ray beam centered at the same positions on various samples showed identical profiles. This observation suggests that x-ray beam exposure of the ESHA-coated mineral samples did not cause changes in the metal-ion distribution during the LP-XSW-FY measurements. However, in order to avoid undetectable changes that might be caused by the x-ray beam, the initial alignment was performed at one position, and each subsequent LP-XSW-FY profile was then collected at a fresh spot after quick realignment to reduce beam exposure. The sample was moved up or down in position at least 1 mm away from the initial alignment position for previous scans. LP-XSW-FY fitting analysis was done using the procedure described in previous studies (Kitts et al., 2009; Levard et al., 2011; Wang et al., submitted-I). The specular x-ray reflectivity was fit using a routine based on Parratt's recursion formula (Parratt, 1954), and was then modeled to obtain the thickness, density, and roughness of the film layer(s) with least-squares fitting. The resulting fit parameters are used to calculate the LP-XSW-FY field intensity modulation. The distribution of the fluorescing species was then obtained by combing the distribution function with the electric field intensity modulation. A two-box model was used in this study which divides the interface into two regions: one near the substrate surface with a thickness of 5 Å and another extending from 5 Å to the top of the ESHA coatings. Attenuation of the emitted fluorescence intensity is accounted for in the LP-XSW-FY calculations. A least-squares routine was used to fit the parameters for the distribution model, from which the element partitioning profiles were obtained. The fitting was performed using custom-made LP-XSW-FY codes in the Igor program (Igor Pro, WaveMetrics, Lake Oswego, Oregon).

3. RESULTS AND DISCUSSION

3.1. Properties and metal-ion contents of ESHA coatings

ESHA contains much higher nitrogen, phosphorous, total amino acid, and total sugar contents compared with the other types of NOMs provided by IHSS (see Table A1). The high content of nitrogen agrees well with the high amount of total amino acid for ESHA, which indicates a high content of N-containing functional groups. The high sugar content of ESHA allows it to form a relatively smooth and uniform film on the metal-oxide surfaces. Fig. 1A shows STXM-based C K-edge NEXAFS spectra for ESHA as compared to SRFA and SRHA. The spectral features at 285.0eV, 286.6eV, and 288.6 eV marked by dashed lines indicate the presence of aromatic, phenolic, and carboxylic functional groups, respectively. The spectrum of the ESHA sample shows a high intensity and broadened peak at ~ 285.0 eV, indicating high aromatic group content. This observation is consistent with the NMR data provided by IHSS, which shows a higher ratio of aromatic (50 ppm) to carboxyl groups (18 ppm) in ESHA as compared with other humic substances such as SRHA and SRFA (IHSS). Humic substances generally contain two major functional groups responsible for metal-ion binding: carboxylic and phenolic functional groups. Titration studies have shown that the p*K*a values for carboxylic groups and phenolic groups in ESHA are 4.36 and 9.8 (IHSS), respectively, which fall in the general range of p*K*a values for these two types of functional groups. However, the concentration of carboxylic groups is much higher than that of phenolic groups in ESHA (see Table A1), suggesting that phenolic groups are not the dominant aromatic groups in ESHA (IHSS). Fig. 1B shows the carbon maps for carboxylic and aromatic carbon of a dry ESHA aggregate. The aromatic part of ESHA appears to be present mostly within the interior of the aggregate, whereas the carboxylic C is distributed throughout the aggregate. This is likely caused by the hydrophobic properties of the aromatic C.

The composition of NOM is very important in metal-ion sequestration because composition is directly related to metal binding properties. The competitive effects between different metal ions due to the presence of a variety of binding sites in humic substances have been studied extensively with several models such as the NICA-Donnan model and Model V and VI (Tipping, 1993; Benedetti et al., 1995; Kinniburgh et al., 1999; Tipping, 2002; Koopal et al., 2005). Three types of interaction between metal ions and NOM can be represented by three different types of sites: (1) non-specific sites due to the electrostatic attraction of cations by abundant negative charges present in humic materials; (2) abundant weak sites including carboxylic and phenolic

342 weak acid groups; and (3) stronger but less abundant sites such as N- and S-containing functional
343 groups. The abundant weak binding sites of humic substances are further divided into stronger
344 phenolic and weaker carboxylic binding sites, which have been extensively studied by
345 experiments as well as modeling (Alberts and Filip, 1998; Tipping, 2002). Certain metal ions
346 such as Al(III) and Pb(II) were found to preferentially bind to phenolic groups, whereas Ca(II),
347 Mg(II), Cd(II), and Fe(II) preferentially bind to carboxylic groups. Others such as Cu(II), Zn(II),
348 Ni(II), and Fe(III) tend to bind to both phenolic and carboxylic groups (Rey-Castro et al., 2009).
349 N- and S-containing groups such as amine and thiol groups in NOM are considered very strong
350 binding sites due to their high affinities for soft metals such as Cu and Hg with log K values > 20
351 (Tipping, 2002). However, knowledge of metal binding with the strongest sites in humic
352 substances is quite limited due to the low concentration of these sites and the lack of suitable
353 analytical techniques for detecting metal speciation at very low metal loadings.
354 LP-XSW-FY has been shown to be a suitable surface characterization technique that can
355 detect elements at trace concentrations (Yoon et al., 2005; Kitts et al., 2009; Levard et al., 2011).
356 Fig. 2 presents a typical fluorescent spectrum collected for ESHA coatings at an incidence angle
357 of 0.1 degree collected at 14 keV incident energy. ESHA as received from IHSS contains various
358 metal ions including Pb, Zn, Cu, Cl, S, Se, Br, Ca, K, Co, Fe, and Ni (LP-XSW-FY spectra of
359 these elements are presented in Fig. A1**)**. Table 1 lists the concentration of Zn, Cu, Fe, K, and Pb
360 in several humic substances analyzed by ICP-AES and the Zn/Cu ratios are compared with those
361 obtained using the LP-XSW-FY technique. Because of the high organic content, ICP-AES is
362 limited to measure NOM solution concentrations of 0.5 g/L or lower. The two measurements
363 show good agreement for Zn/Cu ratio considering that ICP-AES measurements required a 20x
364 dilution and LP-XSW-FY modeling includes a number of corrections for x-ray attenuation.
365 However, LP-XSW-FY method shows a greater sensitivity compared to ICP-AES; our ICP-AES
366 analyses can only detect half of the elements identified by LP-XSW-FY. The amount of Cu(II)
367 ions in ESHA coatings is about 3 times greater than that of Zn(II), whereas Pb(II), Co(II), and
368 Ni(II) are present in trace amounts, which cannot be detected by ICP-AES. Notably, Fe is present
369 in a significant amount in three NOM samples examined (Table 1). The metal-ion content in
370 ESHA coatings is in the order Fe > Cu > Zn > Pb > Co > Ni based on LP-XSW-FY analysis.
371

3.2. Pb(II) partitioning as a function of time between ESHA coatings and α-Al_2O_3 (1-102) single-crystal substrates

Similar to polyacrylic acid (PAA) and biofilm-coated α-Al_2O_3 (1-102) surfaces (Templeton et al., 2001; Yoon et al., 2005; Wang et al., submitted-I), the critical angle of the α-Al_2O_3 (1-102) substrate in the x-ray reflectivity profile is 0.165 ± 0.010 degree at 14 keV incident x-ray energy as shown in Fig. 3. LP-XSW-FY profiles for Pb(II) partitioning as a function of time between ESHA coatings and the α-Al_2O_3 (1-102) substrate are shown in Fig. 4 (10 g/L ESHA, pH = 6.0 ± 0.05, 0.01M $NaNO_3$, [Ca(II)] = 2 mM). Table 2 lists the thickness, roughness, and LP-XSW-FY fitting results for the various samples tested. The thicknesses of the ESHA coatings on the α-Al_2O_3 (1-102) surfaces vary from 250 to 450 nm, depending on the experimental conditions, with roughness ranging from 0.5 to 2.5 nm.

Pb(II) LP-XSW-FY profiles (Fig. 4**)** show two characteristic FY maxima, one at ~ 0.125° (the critical angle of the ESHA) and one at 0.165° ± 0.010 (the critical angle of the α-Al_2O_3 (1-102) surface). The relative intensities of the two maxima in these profiles correlate with the metal-ion distributions in the ESHA coatings and on the α-Al_2O_3 (1-102) surfaces. For samples with short-time equilibration (< 24 hours), the lower angle peak (~ 0.12°) in the LP-XSW-FY profile exhibits a much greater intensity than the higher angle peak (~ 0.165°), which suggests that Pb(II) is mainly sorbed in the ESHA coatings. An increase of the second FY maximum close to the critical angle of α-Al_2O_3 (1-102) surfaces was observed as the reaction time increased, indicating that more Pb(II) ions partitioned onto the Al_2O_3 (1-102) surfaces. Fitting the LP-XSW-FY profiles using two-box model allows extraction of quantitative information regarding the partitioning of Pb(II) between ESHA coatings and the metal-oxide surfaces. Table 2 presents the percentage of Pb(II) onto the α-Al_2O_3 (1-102) surfaces for each reaction time. As the reaction time increased, the percentage of Pb(II) ions on the α-Al_2O_3 (1-102) surfaces increased from 11.4% after 3 hours to 57.4% after 7 days.

Fig. 5 shows the LP-XSW-FY profiles for Cu(II) ions at ESHA-coated α-Al_2O_3 (1-102) surfaces as a function of reaction time. Unlike Pb(II) ions, Cu(II) ions show maxima at ~ 0.125° in the profiles consistently as reaction time increased, suggesting that ESHA coatings dominated the sorption of Cu(II). LP-XSW-FY model fitting results show that more than 99% of Cu(II) ions were associated with ESHA coatings regardless of the reaction time (Table 2). Similar results

have been found for Zn(II) partitioning (see Fig. A2 and Table 2): ESHA coatings dominated Zn sorption (>99%) at all the reaction time tested. It is likely that some Cu(II) and Zn(II) ions partitioned onto the α-Al_2O_3 (1-102) surfaces; however, due to the high concentrations of Cu(II) and Zn(II) ions in ESHA coatings, the two-box model is insensitive so that the amounts of both ions present at α-Al_2O_3 (1-102) surfaces are not resolvable. Similarly, LP-XSW-FY fitting for the other ions present in the systems shows that more than 99% of S, Ca, Cl, Se, Br, Ni, and Co ions are present in the ESHA coatings, and do not show the time dependent partitioning behavior observed for Pb(II) ions.

Fig. 6 shows the percentage of Pb(II) partitioning onto the α-Al_2O_3 (1-102) surface as a function of reaction time. The kinetic data can be divided into two regions: (1) time 0 to 24 hours, and (2) 24 hours to 7 days. An initial rapid increase in the percentage of Pb(II) partitioned onto the α-Al_2O_3 (1-102) surfaces was observed followed by a slower increase. At least two reaction steps are hypothesized in order to explain the reaction kinetics. First, metal ions in the ESHA coatings must dissociate from the metal-humic complex, and then the free metal ions can react with the α-Al_2O_3 (1-102) surfaces as indicated by the following reactions (Hering and Morel, 1988b; Hering and Morel, 1989; Tipping, 2002):

$$\text{Me-A} \rightarrow \text{Me}^{n+} + \text{HA}^{n-} \quad (1)$$

$$\text{Me}^{n+} + \text{M-OH} \rightarrow \text{Me-O-M} + n\text{H}^{+} \quad (2)$$

where Me represents the metal ions, Me-A is the metal ion-humic complex, M-OH is Al- or Fe-(oxy)hydroxide surfaces, Me-O-M is the metal complexes with Al- or Fe-(oxy)hydroxides. The decomplexation/dissociation reaction of metal ions with humic acid is described in reaction 1. Dissociation of monodentate complexes is a hydrolysis reaction, involving displacement of ligand by H_2O (Tipping, 2002). Complexation of metal ions with a mineral surface is described in reaction 2. Redistribution of metal ions from ESHA coatings to the underlying mineral surfaces would be expected if metal ions have a higher affinity for the alumina surface as described by the two simplified reactions. Reaction 2 can occur on time scale of seconds, and is generally fast as compared to reaction 1 (Tipping, 2002; Buffle et al., 2007). Therefore, reaction 1 is the rate-limiting step, especially for strong metal-humic complexes because the rate of

433 dissociation is inversely related to the stability of the complex. The more stable the M-A
434 complex, the slower reaction 1 will be (Tipping, 2002).
435 There are several types of reaction sites present in ESHA coatings as well as on metal-oxide
436 surfaces. The reactive sites in ESHA coatings are known to be heterogeneous, and can be
437 described by a continuous function of affinities or a number of discrete sites. Most models
438 describing metal-humic interactions often use at least three types of binding sites: type A
439 (monodenate site ML type), type B (bidentate site ML_2 type), and type C
440 (tridentate/multidentate, and strong reactive N and S-containing groups) (Benedetti et al., 1995;
441 Kinniburgh et al., 1999; Tipping, 2002; Koopal et al., 2005). Similarly, on the α-Al_2O_3 (1-102)
442 surface, the presence of strong and weak binding sites is also expected (Templeton et al., 2001;
443 Yoon et al., 2005). Thus mobilization of metal ions such as Pb(II) from ESHA coatings to the
444 metal-oxide surfaces may involve multiple reaction steps depending on site densities and binding
445 affinities of the various sites in the ESHA films and on the α-Al_2O_3 (1-102) surfaces, the
446 conformation of the humic molecules, and the physical accessibility of various reactive sites on
447 the surface to metal ions.
448 In general, the densities of type A binding sites are twice as much as type B sites, and the
449 binding affinity of type A sites can be estimated from those of simple carboxylic acids such as
450 acetic and lactic acids. The binding affinity of type B sites (pK_{MHB}) for humic acid, can be
451 predicted from the binding affinity of type A sites (pK_{MHA}) using the relationship: $pK_{MHB} =$
452 $3.0pK_{MHA}-3.0$ (Tipping, 1993; Tipping, 2002). Ephraim et al. (1995) studied 11 aqueous fulvic
453 acids and reported site densities of carboxylic groups to be in the range of 3.72 to 9.86 mmol/g.
454 However, such similarity of metal binding is restricted to the weaker binding sites. Cu, Zn, and
455 Hg are expected to bind preferentially to very strong binding sites such as N-containing groups,
456 and the binding affinities for these sites can vary significantly depending on different sources of
457 humic materials with different N-containing groups and N content (Tipping, 2002). Frenkel et al.
458 (2000) found that Cu binds predominantly with N-containing groups at low metal loadings and
459 pH 4.0, whereas binding to the carboxylic groups dominate at higher metal loadings. Alberts and
460 Filip (1998) concluded that N groups play a more important role than O containing functional
461 groups for Cu(II) binding in humic acid.
462 Although Pb(II) generally has a strong affinity for various functional groups present on
463 bacterial and mineral surfaces (Bargar et al., 1997; Templeton et al., 2001; Bargar et al., 2004;

Ha et al., 2010), the partitioning of Pb(II) from the ESHA coatings to the underlying mineral surface found in the present study suggests that Pb(II) is not as strongly associated with ESHA coatings as Cu(II) and Zn(II). Cu(II) is expected to bind more strongly to functional groups in NOM than Pb(II) due to the affinity of Cu(II) for strong N-containing functional groups in humic acid. Tipping (2002) predicted a "crossover" for Cu(II) and Pb(II) binding in humic acid using Model VI, based on the reasoning that Pb(II) ions have a higher affinity than Cu(II) for the abundant weakly binding sites, but a lower affinity for the more rare strongly binding sites. The difference in metal-ion partitioning behavior observed for Cu(II), Zn(II), and Pb(II) in the present study may be due to the presence of strong binding sites such as N-containing groups in the ESHA coatings. ESHA has considerably higher N content and total amino acids than other IHSS humic acids, as mentioned in section 3.1 (see Table A1). Because the metal ions considered in this study are naturally present in ESHA, they are expected to bind to the strong binding sites of ESHA. Comparison of the Cu(II) and Zn(II) ion concentrations in the ESHA coatings (approximately 0.023% and 0.009%, respectively) with the N concentration in ESHA (4.14%), suggests that these ions bind mostly to N-containing groups in ESHA coatings, and thus should be stable and immobile in the ESHA. We found no evidence that Pb(II) has a strong affinity for N-containing groups; instead, it binds most likely to phenolic groups in humic acid (Rey-Castro et al., 2009). However, the phenolic content of ESHA is quite low compared to the other types of NOMs from IHSS (see Table A1), and it is likely that Pb(II) binds weakly to ESHA. As a result, Pb(II) ions are likely to bind to the strong reactive sites on the underlying α-Al_2O_3 (1-102) surfaces; therefore, Pb(II) is more labile than Cu(II) and Zn(II) under the experimental conditions used here. The weaker binding of Pb(II) by ESHA can also be linked to the low Pb content (~ 0.0002%) of the ESHA coatings in its native state.

Because of their low concentrations, the strong binding sites in humic substances are poorly known (Tipping, 2002; Louis et al., 2009). The low detection limits of the LP-XSW-FY method used in this study allowed us to probe metal concentrations in the nM range. This together with the ability to simultaneously collect fluorescence yield from the different elements present in ESHA opens the possibility of studying metal-ion binding to strong binding sites of NOM as well as competition among the metal ions for the same binding sites in ESHA coatings and the metal-oxide substrates.

3.3. The effect of calcium ions on metal-ion partitioning between ESHA coatings and α-Al_2O_3 (1-102) single-crystal substrates

Because of the abundance of Ca(II) in natural waters, competition between Ca(II) and other metal ions for different binding sites of humic substances and mineral surfaces can be significant (Hering and Morel, 1988a; Hering and Morel, 1988b; Hering and Morel, 1989). For example, Hering and Morel (1988b) found that the kinetics of metal complexation with humic acid can be lowered significantly due to the competition of abundant Ca(II) and Mg(II) with other cations for humic acid binding sites in marine environments. They suggested that, the slow dissociation rate of Ca/Mg-NOM-complexes coupled with these competitive effects are the key factors controlling trace metal reaction kinetics (Hering and Morel, 1988b).

Calcium ions can affect metal ion/humic acid interactions in a number of ways. They can (1) provide charge neutralization of the abundant negatively charged functional groups in humic macromolecules; (2) bind to humic acid at non-specific sites (electrostatic attraction) and weakly complex with the carboxylic groups in humic acids, thus act as a potential major competitor of other metal ions for sorption sites in NOM; (3) increase the ionic strength of the solution more effectively than monovalent ions such as Na and K; and (4) cause bridging between humic molecules, resulting in conformational changes that could lead to physical hindrance of metal binding (Hering and Morel, 1988b; Hering and Morel, 1989; Tipping, 2002). The effect of Ca(II) ions on metal-humic binding is an intricate interplay of these factors. Therefore, it is important to consider the kinetics of metal ion-humic acid complexation/dissociation perturbed by the addition of metal ions such as Ca(II).

Cu(II), Zn(II), and Pb(II) partitioning between EHSA coatings and the α-Al_2O_3 (1-102) substrates in the system without the addition of calcium were measured (see Fig. A3) and the metal-ion partitioning results were presented in Table 2. Fig. 6 shows the influence of Ca(II) ions on Pb(II) and Cu(II) partitioning as a function of reaction time. Similar to the system with added Ca, the partitioning of Pb(II) to the α-Al_2O_3 (1-102) surfaces increased as reaction time increased, suggesting that Pb(II) increasingly mobilized to the reactive α-Al_2O_3 (1-102) surfaces. From the initial reaction to about 24 hrs, the addition of 2 mM Ca(II) ions to the system did not show much difference in Pb(II) partitioning to the α-Al_2O_3 (1-102) surfaces. However, for longer

reaction times (from 2 days to 7 days), we observed a slightly higher Pb(II) partitioning to the α-Al_2O_3 (1-102) surfaces in the presence of 2 mM Ca relative to the system without Ca.

The slightly enhanced partitioning of Pb(II) ions to Al_2O_3 (1-102) surfaces in the 2 mM calcium system at longer reaction time indicates that Ca(II) ions compete with Pb(II) for binding sites in ESHA coatings, i.e. large amounts of introduced Ca(II) ions replaced weakly bound Pb(II) in the ESHA and increased the amount of Pb(II) redistributed to the α-Al_2O_3 (1-102) surface. Competitive sorption effects of Ca(II) on Cu(II) and Cd(II) binding by humic acid have been studied by Kinniburgh et al. (1999). Ca(II) was reported to compete much more effectively with Cd(II) for the low affinity sites (carboxylic groups) than with Cu(II) for high affinity sites (phenolic and N- or S-containing groups) (Kinniburgh et al., 1999). The effect of Ca(II) on Cd(II) binding was found to be significant, but almost no effect of Ca(II) was observed for Cu(II) binding to humic acids (Tipping, 2002).

On the other hand, increasing Ca concentration increased the ionic strength which promotes electrostatic shielding and deceases metal binding in humic substances. Although ionic strength does not play a major role in controlling inner-sphere complexation reactions, it becomes an important parameter for metal-ion sorption on highly negatively charged humic molecules, especially for weaker binding sites. Metal-ion binding to humic acids has been shown to decrease with increasing ionic strength (Fitch et al., 1986; Zachara and Smith, 1994). NICCA-Donnan model predicted that the effect of ionic strength is more pronounced for Pb(II) than Cu(II) (Tipping, 2002). In our case, Pb(II) binding by ESHA is weakened by competition with Ca(II) and increasing ionic strength; therefore, more Pb(II) is redistributed to the α-Al_2O_3 (1-102) surfaces compared to the systems without added Ca.

In addition, Ca(II) has been found to increase the aggregation of humic macromolecules, and increase the adsorption of humic acids to iron-oxide surfaces (Tipping, 2002). In our study, the film-air roughness was always higher in all the samples with 2 mM Ca added compared to the systems without Ca (Table 2). This finding is likely due to the fact that addition of Ca(II) ions causes more aggregation of the macromolecules in the ESHA coatings. The well-known bridging effect of Ca(II) on humic acid can cause steric interference or physical hindrance for Pb(II) ions to be released from humic acid which could partially explain why the effect of Ca(II) competition with Pb(II) binding by humic acid in our study was not obvious during the initial 24 hours of reaction.

Another possible explanation for the observed higher Pb(II) mobility in the 2 mM calcium system is the fact that adding Ca(II) ions and then filtering the ESHA solution though 0.22 μm filters removed the larger and more hydrophobic fraction of ESHA. This fraction of humic acid is often associated with aromatic functional groups and possibly phenolic groups, which are likely to be the stronger binding sites for Pb(II) ions in the ESHA coatings. Hence, Pb(II) ions left in the ESHA solutions are more weakly bound, and are therefore more likely to be mobilized to the metal-oxide surfaces once in contact with strong sorption sites on these surfaces.

3.4. Metal-ion partitioning between ESHA coatings and α-Al_2O_3 (0001) and α-Fe_2O_3 (0001) single crystal surfaces

Short time (3-hour) and long time (3-day) samples were collected for ESHA-coated α-Al_2O_3 (0001) and α-Fe_2O_3 (0001) single-crystal surfaces samples. X-ray reflectivity curves collected for the ESHA-coated α-Al_2O_3 (0001) surfaces (see Fig. 3 and Fig. A4) are similar to those for ESHA-coated α-Al_2O_3 (1-102) surfaces, with a critical angle of 0.165 ± 0.010 degree at 14 keV of incident x-ray energy. ESHA coatings formed on α-Al_2O_3 (0001) surfaces are generally thinner (200-270 nm) than ESHA coatings formed on α-Al_2O_3 (1-102) surfaces (Table 3). Unlike the α-Al_2O_3 (1-102) surface, Cu(II), Zn(II), and Pb(II) present in the ESHA coatings on the α-Al_2O_3 (0001) surface do not show time-dependent partitioning from the coatings to the surface (see Fig. A4 and Table 3). More than 99% of the Pb(II), Cu(II), Zn(II), Ni(II), Co(II), S, Fe, P, Se, Cl and Br ions remained in the ESHA coatings even after 3 days of reaction. This finding is consistent with the fact that α-Al_2O_3 (0001) is a relatively inert surface as shown in previous studies (Liu et al., 1998; Templeton et al., 2001; Yoon et al., 2005).

Reflectivity profiles collected for ESHA-coated α-Fe_2O_3 (0001) surfaces (see Fig. 3 and Fig. A5) show the critical angle of the substrate is 0.185° ± 0.010 at 14 keV of incident x-ray energy. ESHA coatings formed on α-Fe_2O_3 (0001) surfaces are generally thicker (349.2 nm after 3 hours of reaction to 542.0 nm after 3 days of reaction) than those formed on the α-Al_2O_3 (0001) and (1-102) surfaces (Table 3). Significant amounts of Pb(II) ions quickly redistributed to the α-Fe_2O_3 (0001) surface after 3 hours (74.1%) and increasingly partitioned to the surface after 3 days of reaction (91.7%) (see Table 3 and Fig. A5**)**. These changes indicate that the α-Fe_2O_3 (0001) surface is much more reactive to Pb(II) compared with the α-Al_2O_3 (1-102) surfaces. Templeton

et al. (2001) showed that the site densities of the strong binding sites on the α-Fe_2O_3 (0001) surface are about 2.5 times higher than those on the α-Al_2O_3 (1-102) surfaces, and Pb(II) binding affinities to the strong binding sites on α-Fe_2O_3 (0001) are about 4.5 times higher than those on α-Al_2O_3 (1-102) surfaces (Templeton et al., 2001). As a result, Pb(II) was quickly mobilized from the ESHA coatings to the more reactive α-Fe_2O_3 (0001) surface. In contrast to Pb(II), both Cu(II) and Zn(II) ions showed almost no partitioning from the ESHA coatings to the α-Al_2O_3 (0001) and (1-102) surfaces with respect to reaction time (> 99% of the ions were in the ESHA coatings). However, even Cu(II) ions showed a slight partitioning (2.4%) to the α-Fe_2O_3 (0001) surface after 3 hours of reaction and continuously increased to 6.4% after 3 days even though Cu(II) ions have much higher concentrations in the ESHA coatings compared with that of Pb(II) ions. Similarly, 3.7% of Zn(II) ions partitioned to the α-Fe_2O_3 (0001) surface after 3 hours and 7.7% of Zn(II) ions partitioned to the α-Fe_2O_3 (0001) surface after 3 days.

Table 3 compares the partitioning of Pb(II), Cu(II), and Zn(II) ions between ESHA coatings and the three mineral surfaces: α-Al_2O_3 (0001), α-Al_2O_3 (1-102), and α-Fe_2O_3 (0001). For the inert α-Al_2O_3 (0001) surfaces, the ESHA coatings were the dominant sinks for all three metal ions regardless of the reaction time. For the α-Al_2O_3 (1-102) surfaces, only Pb(II) ions showed significant partitioning to the surface after 3 hours, and the surfaces dominated Pb(II) sorption after 7 days for the system with added calcium. For the α-Fe_2O_3 (0001) surfaces, all three metal ions migrated toward the surface after 3 hours, and the partitioning continued to increase after 3 days of exposure time. Therefore, the α-Fe_2O_3 (0001) surface is the most reactive surface towards metal ions, followed by the α-Al_2O_3 (1-102) and α-Al_2O_3 (0001) surfaces.

Past studies have shown that the mode of binding and mechanism of formation of metal-ion sorption complexes formed on at metal-oxide/water interfaces are strongly dependent on the orientation, composition, and structure of the surfaces (Bargar et al., 1996; Bargar et al., 1997; Trainor et al., 2000; Trainor et al., 2001; Bargar et al., 2004). For example, Pb(II) sorption complexes formed on alumina surfaces are sensitive to the crystallographic orientation and sorption density: Pb(II) forms primarily outer-sphere complexes on α-Al_2O_3 (0001) surfaces (Bargar et al., 1996), but it forms a variety of inner-sphere complexes (mononuclear at low sorption to multinuclear at high sorption density) on α-Al_2O_3 (1-102) surfaces (Bargar et al., 1997; Bargar et al., 2004). In contrast, Pb(II) forms dominantly inner-sphere complexes on both the (0001) and (1-102) surfaces of α-Fe_2O_3 (Bargar et al., 2004). On the other hand, Zn(II)

forms predominantly inner-sphere complexes on both the (0001) and (1-102) surfaces of α-Al_2O_3 (Trainor et al., 2001). A general trend in reactivity exists among three model surfaces with respect to reactivity with metal ions: α-Fe_2O_3 (0001) > α-Al_2O_3 (1-102) > α-Al_2O_3 (0001), as shown in various metal sorption studies on clean uncoated surfaces as well as on biofilm- and PAA-coated surfaces (Liu et al., 1998; Templeton et al., 2001; Yoon et al., 2005; Wang et al., submitted-I). The reactivity of surfaces with respect to metal-ion sorption observed in this study is consistent with this general trend. Thus, we conclude that the intrinsic order of reactivity of the metal-oxide surface is preserved even with 200-500 nm thick, dense ESHA coatings, suggesting that the ESHA coatings do not block reactive sites on the metal-oxide surfaces.

3.5. The effect of pH on metal-ion partitioning between ESHA coatings and α-Al_2O_3 (1-102) single crystal surfaces

ESHA film thickness, roughness, and the percentage of Pb(II) ions in the ESHA coatings and on the surfaces as a function of pH are reported in Table 3. As the pH was increased from 4.0 to 9.0, the reflectivity profiles changed significantly, which indicates that the ESHA film properties changed (see Fig. A6). At pH 4.0 and 9.0, the ESHA coatings were much rougher (~ 45 and ~ 24 Å rms roughness, respectively) compared with the coatings formed at pH 6.0 (~ 10 Å rms roughness). These differences in roughness suggest that the ESHA macromolecules in the coatings may have undergone conformational change as pH changed. Such changes in the conformation of fulvic acid in solution have been previously observed using transmission x-ray microscopy (Myneni et al., 1999). Solution chemistry, including pH and ionic strength, has a profound influence on the size and conformation of NOM molecules causing its structural complexity (Myneni et al., 1999). At pH 4.0, both carboxylic (pK_a = 4.3) and phenolic (pK_a = 9.8) functional groups are protonated and thus ESHA has a relatively low negative charge. In this case, ESHA macromolecules tend to aggregate due to their low electrostatic repulsive interactions (Tipping, 2002). Aggregate formation could lead to the high roughness observed for the ESHA coatings at pH 4.0. However, ESHA macromolecules can still be easily attached to α-Al_2O_3 (1-102) surfaces because the surface has a positive charge at pH 4.0. The pH_{PZC} of α-Al_2O_3 (1-102) single-crystal surfaces was found to be 5.2 for α-Al_2O_3 (1-102) (Wang et al., submitted-II). At pH 9.0, most of the functional groups of ESHA are deprotonated and have

649 significant negative charges, thus molecules tend to be more linear, flexible chains instead of
650 coils, and fewer aggregates will be formed in the ESHA coatings as compared with pH values of
651 4.0 and 6.0. On the other hand, the surface of α-Al_2O_3 (1-102) has a negative charge at pH 9.0,
652 and the attachment of the ESHA coatings is expected to be more difficult at this pH values as
653 compared with pH 4.0 and 6.0. Based on the above reasoning, the film formed at pH 6.0 should
654 have the lowest roughness compared with the films formed at pH 4.0 and 9.0.
655 LP-XSW-FY fitting results show that Pb(II) partitioning increased from ~ 4% to ~ 55% as
656 pH is increased from 4.0 to 9.0 (see Table 3 and Fig. A6). Similar to the observed changes in
657 film roughness discussed above, the increased partitioning of Pb(II) to the α-Al_2O_3 (1-102)
658 surface at higher pH can also be attributed to changes of the electrostatic interactions of both the
659 ESHA coatings and the α-Al_2O_3 (1-102) surface. At pH 4.0, the surface of α-Al_2O_3 (1-102) has a
660 positive charge compared to ESHA, and therefore positively charged Pb(II) ions have a higher
661 affinity for the negatively charged ESHA, resulting in ~ 96% of the Pb(II) being associated with
662 the ESHA coatings, as shown in Table 3. On the other hand, the charge of α-Al_2O_3 (1-102)
663 surface tends to be more negative and has a more attractive interaction with Pb(II) cations as pH
664 increases; thus sorption of Pb(II) ions on the α-Al_2O_3 (1-102) surface becomes more favorable.
665
666 **4. CONCLUSIONS**
667
668 Partitioning of Cu(II), Zn(II), and Pb(II) ions between ESHA coatings and Al- and Fe-oxide
669 substrates was studied using the LP-XSW-FY technique as a function of reaction time, pH, and
670 calcium content. More than 15 different naturally present elements were detected in the ESHA
671 coatings, some of which had concentrations higher than 0.05% by weight (Fe, K, S, and P). The
672 concentrations of Cu(II), Zn(II), and Pb(II) in the ESHA coatings were much lower (~0.023%,
673 ~0.009%, and ~0.0002%, respectively). Unlike Cu(II) and Zn(II) ions, Pb(II) ions partitioned
674 strongly from the ESHA coatings to reactive sites on the α-Al_2O_3 (1-102) and α-Fe_2O_3 (0001)
675 surfaces, suggesting weak binding of Pb(II) to ESHA functional groups as compared to Cu(II)
676 and Zn(II) ions, which are likely associated with strong N-containing sites in ESHA coatings.
677 Adding calcium to the ESHA/α-Al_2O_3(1-102) system slightly increased Pb(II) partitioning to the
678 α-Al_2O_3 (1-102) surfaces at longer reaction time possibly due to the competitive binding effects
679 of calcium. The partitioning of Pb(II) to the α-Al_2O_3(1-102) surfaces was also found to increase

with increasing pH due to enhanced electrostatic attraction resulting from the increasing negative charge of these surfaces. The intrinsic order of reactivity of three metal-oxide surfaces was found to be α-Fe_2O_3 (0001) > α-Al_2O_3 (1-102) > α-Al_2O_3 (0001) in spite of the presence of ESHA coatings. This order of reactivity is the same as that of the bare surfaces with respect to metal-ion adsorption. The LP-XSW-FY technique is a promising analytical tool for probing strong binding sites of NOMs as well as for studying competitive effects of different metal ions at complex environmental interfaces. This study provides new insights into the binding affinity, reaction mechanisms, and reaction kinetics of Pb(II), Cu(II), and Zn(II) with common soil organic matter and common Fe- and Al-oxide surfaces. Our results shed new light on the potential bioavailability of these metal contaminants in soils and natural aquatic systems containing humic materials and common metal oxides.

ACKNOWLEDGMENTS

This study was supported by NSF Grant CHE-0431425 (Stanford Environmental Molecular Science Institute). The LP-XSW-FY data reported in this paper were collected at GeoSoilEnviroCARS (Advanced Photon Source Sector 13) at the Advanced Photon Source, Argonne National Laboratory. GeoSoilEnviroCARS is supported by the National Science Foundation - Earth Sciences (EAR-0622171) and the Department of Energy - Geosciences (DE-FG02-94ER14466). The Advanced Photon Source is supported by the U. S. Department of Energy, Office of Science, Office of Basic Energy Sciences, under Contract No. DE-AC02-06CH11357. We wish to thank Guangchao Li (Stanford University) for ICP-AES analysis. The STXM data reported in this paper were collected at the Advanced Light Source, Lawrence Berkeley National Laboratory. The Advanced Light Source is supported by the Director, Office of Science, Office of Basic Energy Sciences, of the U.S. Department of Energy under Contract No. DE-AC02-05CH11231.

REFERENCES

Abruna H. D., White J. H., Bommarito G. M., Albarelli M. J., Acevedo D. and Bedzyk M. J. (1989) Structural studies of electrochemical interfaces with x-rays. *Rev. Sci. Instruments* **60**, 2529-2532.

712 Aiken G. and Cotsaris E. (1995) Soil and Hydrology - Their effect on NOM. *J. Am. Water Work*
713 *Assoc.* **87**, 36-45.
714 Alberts J. J. and Filip Z. (1998) Metal binding in estuarine humic and fulvic acids: FTIR analysis
715 of humic acid-metal complexes. *Environ. Technol.* **19**, 923-931.
716 Au K. K., Penisson A. C., Yang S. L. and O'Melia C. R. (1999) Natural organic matter at
717 oxide/water interfaces: Complexation and conformation. *Geochim. Cosmochim. Acta* **63**,
718 2903-2917.
719 Balistrieri L., Brewer P. G. and Murray J. W. (1981) Scavenging residence times of trace metals
720 and surface chemistry of sinking particles in the deep ocean. *Deep-Sea Res.* **28A**, 101-
721 121.
722 Bargar J. R., Brown, Jr., G. E. and Parks G. A. (1997) Surface complexation of Pb(II) at oxide-
723 water interfaces. 2. XAFS and bond-valence determination of mononuclear Pb(II)
724 sorption products and surface functional groups on iron oxides. *Geochim. Cosmochim.*
725 *Acta* **61**, 2639-2652.
726 Bargar J. R., Towle S. N., Brown, Jr., G. E. and Parks G. A. (1996) Outer-sphere Pb(II) adsorbed
727 at specific surface sites on single crystal α-alumina. *Geochim. Cosmochim. Acta* **60**,
728 3541-3547.
729 Bargar J. R., Trainor T. P., Fitts J. P., Chambers S. A. and Brown, Jr., G. E. (2004) In situ
730 grazing-incidence extended x-ray absorption fine structure study of Pb(II) chemisorption
731 on hematite (0001) and (1-102) surfaces. *Langmuir* **20**, 1667-1673.
732 Batterman B. W. (1964) Effect of dynamical diffraction in x-ray fluorescence scattering. *Phys.*
733 *Rev. A-Gen. Phys.* **133**, A759-764.
734 Batterman B. W. and Cole H. (1964) Dynamical diffraction of x-rays by perfect crystals. *Rev.*
735 *Mod. Phys.* **36**, 681-717.
736 Bedzyk M. J. (1992) X-ray standing wave studies of the liquid/solid interface and ultrathin
737 organic films. In: *Surface X-ray and Neutron Scattering. Springer Proceedings in Physics*
738 (Eds. Zabel., H. and Robinson, I. K.) Spronger-Verlag, Berlin, pp. 113-117.
739 Bedzyk M. J., Bilderback D. H., White J., Abruna H. D. and Bommarito M. G. (1986) Probing
740 electrochemical interfaces with x-ray standing waves. *J. Phys. Chem.* **90**, 4926-4928.
741 Bedzyk M. J., Bilderback D. H., Bommarito G. M., Caffrey M. and Schildkraut J. S. (1988) X-
742 ray standing waves - a molecular yardstick for biological-membranes. *Science* **241**, 1788-
743 1791.
744 Bedzyk M. J., Bommarito G. M., Caffrey M. and Penner T. L. (1990) Diffuse-double layer at a
745 membrane-aqueous interface measured with x-ray standing waves. *Science* **248**, 52-56.
746 Bedzyk M. J. and Cheng L. (2002) X-ray standing wave studies of minerals and mineral
747 surfaces: Principles and applications. In: *Applications of Synchrotron Radiation in Low-*
748 *Temperature Geochemistry and Environmental Science*. (Eds. Fenter, P.A., Rivers M.L.,
749 Sturchio N.C., Sutton, S.R.) *Rev. Mineral. Geochem.*, **49**, Washington D.C., pp. 221-266.
750 Benedetti M. F., Milne C. J., Kinniburgh D. G., van Riemsdijk W. H. and Koopal L. K. (1995)
751 Metal-ion binding to humic substances - application of the nonideal competitive
752 adsorption model. *Environ. Sci. Technol.* **29**, 446-457.
753 Bonneville, S., Smits, M. M., Brown, A., Harrington, J., Leake, J. R., Brydson, R. and Benning
754 L. G. (2012) Plant-driven fungal weathering: early stages of mineral alteration at the
755 nanometer scale. *Geology* **37(7)**, 615-618.

Buffle J., Zhang Z. and Startchev K. (2007) Metal flux and dynamic speciation at (bio)interfaces. part 1: Critical evaluation and compilation of physicochemical parameters for complexes with simple Ligands and Fulvic/Humic substances. *Environ. Sci. Technol.* **41**, 7609-7620.

Cowan P. L., Golovchenko J. A. and Robbins M. F. (1980) X-ray standing waves at crystal-surfaces. *Phys. Rev. Lett.* **44**, 1680-1683.

Davis J. A. (1984) Complexation of trace-metals by adsorbed natural organic-matter. *Geochim. Cosmochim. Acta* **48**, 679-691.

Eng P. J., Trainor T. P., Brown, Jr., G. E., Waychunas G. A., Newville M., Sutton S. R. and Rivers M. L. (2000) Structure of the hydrated α-Al_2O_3 (0001) surface. *Science* **288**, 1029-1033.

Ephraim J. H., Pettersson C., Norden M. and Allard B. (1995) Potentiometric titrations of humic substances - do ionic-strength effects depend on the molecular-weight? *Environ. Sci. Technol.* **29**, 622-628.

Fitch A., Stevenson F. J. and Chen Y. (1986) Complexation of Cu(II) with a soil humic-acid - response characteristics of the Cu(II) ion-selective electrode and ligand concentration effects. *Organic Geochem.* **9**, 109-116.

Frenkel A. I., Korshin G. V. and Ankudinov A. L. (2000) XANES study of Cu^{2+}-binding sites in aquatic humic substances. *Environ. Sci. Technol.* **34**, 2138-2142.

Golovchenko J. A., Batterman B. W. and Brown W. L. (1974) Observation of internal x-ray wave fields during bragg-diffraction with an application to impurity lattice location. *Phys. Rev. B* **10**, 4239-4243.

Gu B., Mehlhorn T. L., Liang L. and McCarthy J. F. (1996a) Competitive adsorption, displacement, and transport of organic matter on iron oxide: I. Competitive adsorption. *Geochim. Cosmochim. Acta* **60**, 1943-1950.

Gu B., Mehlhorn T. L., Liang L. and McCarthy J. F. (1996b) Competitive adsorption, displacement, and transport of organic matter on iron oxide: II. Displacement and transport. *Geochim. Cosmochim. Acta* **60**, 2977-2992.

Ha J., Gelabert A., Spormann A. M. and Brown, Jr., G. E. (2010) Role of extracellular polymeric substances in metal ion complexation on *Shewanella oneidensis*: Batch uptake, thermodynamic modeling, ATR-FTIR, and EXAFS study. *Geochim. Cosmochim. Acta* **74**, 1-15.

Herbert B. E. and Bertsch P. M. (1995) Characterization of dissolved and colloidal organic matter in soil solution: a review. In: *Carbon forms and functions in forest soils* (Eds. McFee, W. W. and Kelly, J. M.). Soil Science Society of America, Madison, Wisconsin, USA. pp. 63-88.

Hering J. G. and Morel F. M. M. (1988a) Humic-acid complexation of calcium and copper. *Environ. Sci. Technol.* **22**, 1234-1237.

Hering J. G. and Morel F. M. M. (1988b) Kinetics of trace-metal complexation - role of alkaline-earth metals. *Environ. Sci. Technol.* **22**, 1469-1478.

Hering J. G. and Morel F. M. M. (1989) Slow coordination reactions in seawater. *Geochim. Cosmochim. Acta* **53**, 611-618.

Hitchcock A. P. (2000) AXis2000 software (ver2.1n). *http://unicorn.mcmaster.ca/aXis2000.html.*

IHSS http://www.humicsubstances.org/.

Kinniburgh D. G., van Riemsdijk W. H., Koopal L. K., Borkovec M., Benedetti M. F. and Avena M. J. (1999) Ion binding to natural organic matter: competition, heterogeneity, stoichiometry and thermodynamic consistency. *Colloids Surf. A* **151**, 147-166.

Kitts K., Choi Y., Eng P. J., Ghose S. K., Sutton S. R. and Rout B. (2009) Application of grazing incidence x-ray fluorescence technique to discriminate and quantify implanted solar wind. *J. Appl. Phys.* **105**, 064905(1-3).

Koopal L. K., Saito T., Pinheiro J. P. and van Riemsdijk W. H. (2005) Ion binding to natural organic matter: General considerations and the NICA-Donnan model. *Colloids Surf. A* **265**, 40-54.

Lalonde K., Mucci A., Ouellet A. and Gelinas Y. (2012) Preservation of organic matter in sediments promoted by iron. *Nature* **483**, 198-200.

Leenheer J., McKnight D., Thurman E. and MacCarthy P. (1994) Humic Substances in the Suwannee River, Georgia: Interactions, Properties, and Proposed Structures (Eds. Averett, R. C., Leenheer, J.A., McKnight, D.M., Thorn, K.A.) U.S. Geological Survey, Denver, CO. pp. 195-211.

Levard C., Michel F. M., Wang Y. G., Choi Y., Eng P. J. and Brown, Jr., G. E. (2011) Probing Ag nanoparticle surface oxidation in contact with (in)organics: an x-ray scattering and fluorescence yield approach. *J. Synchrot. Radiat.* **18**, 871-878.

Liu P., Kendelewicz T., Brown, Jr., G. E., Nelson E. J. and Chambers S. A. (1998) Reaction of water vapor with α-Al_2O_3(0001) and α-Fe_2O_3(0001) surfaces: synchrotron x-ray photoemission studies and thermodynamic calculations. *Surf. Sci.* **417**, 53-65.

Lofts S., Simon B. M., Tipping E. and Woof C. (2001) Modelling the solid-solution partitioning of organic matter in European forest soils. *Eur. J. Soil Sci.* **52**, 215-226.

Louis Y., Garnier C., Lenoble V., Mounier S., Cukrov N., Omanovic D. and Pizeta I. (2009) Kinetic and equilibrium studies of copper-dissolved organic matter complexation in water column of the stratified Krka River estuary (Croatia). *Mar. Chem.* **114**, 110-119.

Mayer L. M. (1994) Surface-area control of organic-carbon accumulation in continental-shelf sediments. *Geochim. Cosmochim. Acta* **58**, 1271-1284.

Mayer L. M. (1999) Extent of coverage of mineral surfaces by organic matter in marine sediments. *Geochim. Cosmochim. Acta* **63**, 207-215.

Mayer L. M. and Xing B. S. (2001) Organic matter-surface area relationships in acid soils. *Soil Sci. Soc. Am. J.* **65**, 250-258.

Myneni S. C. B., Brown J. T., Martinez G. A. and Meyer-Ilse W. (1999) Imaging of humic substance macromolecular structures in water and soils. *Science* **286**, 1335-1337.

Neihof R. and Loeb G. (1974) Dissolved organic-matter in seawater and electric charge of immersed surfaces. *J. Mar. Res.* **32**, 5-12.

Parratt L. G. (1954) Solid surface studies by total reflection of x-rays. *Phys. Rev.* **95**, 617-617.

Pingitore N. E., Clague J. W., Amaya M. A., Maciejewska B. and Reynoso J. J. (2009) Urban airborne lead: x-ray absorption spectroscopy establishes soil as dominant source. *PLOS One* **4**(4)**,** e5019.

Ransom B., Bennett R. H., Baerwald R. and Shea K. (1997) TEM study of in situ organic matter on continental margins: Occurrence and the "monolayer" hypothesis. *Mar. Geol.* **138**, 1-9.

Rey-Castro C., Mongin S., Huidobro C., David C., Salvador J., Lluis Garces J., Galceran J., Mas F. and Puy J. (2009) Effective affinity distribution for the binding of metal ions to a generic fulvic acid in natural waters. *Environ. Sci. Technol.* **43**, 7184-7191.

Tanwar K. S., Lo C. S., Eng P. J., Catalano J. G., Walko D. A., Brown, Jr., G. E., Waychunas G. A., Chaka A. M. and Trainor T. P. (2007) Surface diffraction study of the hydrated hematite (1-102) surface. *Surf. Sci.* **601**, 460-474.

847 Templeton A. S., Trainor T. P., Spormann A. M. and Brown, Jr., G. E. (2003) Selenium
848 speciation and partitioning within *Burkholderia cepacia* biofilms formed on α-Al_2O_3
849 surfaces. *Geochim. Cosmochim. Acta* **67**, 3547-3557.
850 Templeton A. S., Trainor T. P., Traina S. J., Spormann A. M. and Brown, Jr., G. E. (2001) Pb(II)
851 distributions at biofilm-metal oxide interfaces. *Proc. Natl. Acad. Sci. U. S. A.* **98**, 11897-
852 11902.
853 Thurman E.M. W., R.L. Malcolm and D.J. Pinckney (1982) Molecular size of aquatic humic
854 substances. *Org. Geochem.* **4**, 27-35.
855 Tipping E. (1993) Modeling ion-binding by humic acids. *Colloids Surf. A* **73**, 117-131.
856 Tipping E. (2002). *Cation Binding by Humic Substances*. Cambridge University Press,
857 Cambridge, U.K., pp. 4-31.
858 Tipping E., Rey-Castro C., Bryan S. E. and Hamilton-Taylor J. (2002) Al(III) and Fe(III) binding
859 by humic substances in freshwaters, and implications for trace metal speciation.
860 *Geochim. Cosmochim. Acta* **66**, 3211-3224.
861 Tombacz E., Libor Z., Illes E., Majzik A. and Klumpp E. (2004) The role of reactive surface
862 sites and complexation by humic acids in the interaction of clay mineral and iron oxide
863 particles. *Org. Geochem.* **35**, 257-267.
864 Trainor T. P., Brown, Jr., G. E. and Parks G. A. (2000) Adsorption and precipitation of aqueous
865 Zn(II) on alumina powders. *J. Colloid Interface Sci.* **231**, 359-372.
866 Trainor T. P., Chaka A. M., Eng P. J., Newville M., Waychunas G. A., Catalano J. G. and
867 Brown, Jr., G. E. (2004) Structure and reactivity of the hydrated hematite (0001) surface.
868 *Surf. Sci.* **573**, 204-224.
869 Trainor T. P., Eng P. J., Brown, Jr., G. E., Robinson I. K. and De Santis M. (2002) Crystal
870 truncation rod diffraction study of the α-Al_2O_3 (1-102) surface. *Surf. Sci.* **496**, 238-250.
871 Trainor T. P., Fitts J. P., Templeton A. S., Grolimund D. and Brown, Jr., G. E. (2001) Grazing-
872 incidence XAFS study of aqueous Zn(II) sorption on α-Al_2O_3 single crystals. *J. Colloid*
873 *Interface Sci.* **244**, 239-244.
874 Trainor T. P., Templeton A. S. and Eng P. J. (2006) Structure and reactivity of environmental
875 interfaces: Application of grazing angle x-ray spectroscopy and long-period x-ray
876 standing waves. *J. Electron Spectrosc. Relat. Phenom.* **150**, 66-85.
877 Van Riemsdijk W. H., Koopal L. K., Kinniburgh D. G., Benedetti M. F. and Weng L. (2006)
878 Modeling the interactions between humics, ions, and mineral surfaces. *Environ. Sci.*
879 *Technol.* **40**, 7473-7480.
880 Wang J., Bedzyk M. J. and Caffrey M. (1992) Resonance-enhanced x-rays in thin-films - a
881 structure probe for membranes and surface-layers. *Science* **258**, 775-778.
882 Wang J., Bedzyk M. J., Penner T. L. and Caffrey M. (1991) Structural studies of membranes and
883 surface-layers up to 1,000 a thick using x-ray standing waves. *Nature* **354**, 377-380.
884 Wang Y., Gélabert A., Michel F. M., Choi Y., Gesher G., Eng P. J., Bargar J. R., Onagema G.,
885 Spormann A. M. and Brown, Jr., G. E. (submitted-I) Effect of biofilm coatings at metal-
886 oxide/water interfaces I: Pb(II) and Zn(II) partitioning and speciation at *Shewanella*
887 *oneidensis*/metal-oxide/water interfaces. *Geochim. Cosmochim. Acta*.
888 Wang Y., Walewijk S., Michel F. M., Persson P. and Brown, Jr., G. E. (submitted-II)
889 Comparison of isoelectric points of single crystal and particulate α-Al_2O_3 and α-Fe_2O_3
890 surfaces. *Geochim. Cosmochim. Acta*.
891 Wightman P. G. and Fein J. B. (2001) Ternary interactions in a humic acid-Cd-bacteria system.
892 *Chem. Geol.* **180**, 55-65.

Yoon T. H., Trainor T. P., Eng P. J., Bargar J. R. and Brown, Jr., G. E. (2005) Trace metal ion partitioning at polymer film-metal oxide interfaces: Long-period x-ray standing wave study. *Langmuir* **21**, 4503-4511.

Zachara J. R., CT; Smith, SC (1994) Influence of humic substances on Co^{2+} sorption by a subsurface mineral separate and its mineralogic components. *Geochim. Cosmochim. Acta* **58**, 553-566.

Table 1. ICP-AES analysis results for metal concentrations in 0.5 g/L NOM solutions and comparison of Zn/Cu ratios determined by ICP-AES and LP-XSW-FY analysis.

Type of NOM	Zn (ppb)	Cu (ppb)	Fe (ppb)	K (ppb)	Phosphorus (ppb)	ICP-AES (Zn/Cu)	LP-XSW-FY (Zn/Cu)
SRFA	50.7	8.0	159.4	174.3	24.3	6.35	6.02
SRHA	114.2	9.1	529.9	213.9	40.6	12.53	13.11
ESHA	45.0	113.4	405.8	815.9	566.8	0.388	0.324

Table 2. Results from x-ray reflectivity and LP-XSW-FY analyses of the partitioning of Pb(II), Cu(II), and Zn(II) between ESHA coatings and α-Al_2O_3(1-102) surfaces (pH = 6.0±0.05, ESHA concentration = 10g/L, 0.01M $NaNO_3$).

Metal-oxide surface	Time (hours)	Added [Ca(II)]	Film thickness (Å)	Film-air interface roughness (Å)	Pb% on the surface	Cu% on the surface	Zn% on the surface
α-Al_2O_3(1-102)	0	-	416.0	8.2	<1	<1	<1
α-Al_2O_3(1-102)	3	-	322.9	8.4	13.6	<1	<1
α-Al_2O_3(1-102)	12	-	387.1	9.0	16.2	<1	<1
α-Al_2O_3(1-102)	24	-	303.4	7.7	20.1	<1	<1
α-Al_2O_3(1-102)	48	-	360.2	9.1	33.9	<1	<1
α-Al_2O_3(1-102)	72	-	325.8	9.9	39.8	<1	<1
α-Al_2O_3(1-102)	168	-	453.2	12.0	46.1	<1	<1
α-Al_2O_3(1-102)	0	$2*10^{-3}$M	266.6	17.4	4.0	<1	<1
α-Al_2O_3(1-102)	3	$2*10^{-3}$M	333.8	16.3	11.4	<1	<1
α-Al_2O_3(1-102)	12	$2*10^{-3}$M	281.3	11.2	13.2	<1	<1
α-Al_2O_3(1-102)	24	$2*10^{-3}$M	391.6	23.7	21.5	<1	<1
α-Al_2O_3(1-102)	48	$2*10^{-3}$M	421.8	20.9	40.0	<1	<1
α-Al_2O_3(1-102)	72	$2*10^{-3}$M	344.6	23.1	58.3	<1	<1
α-Al_2O_3(1-102)	168	$2*10^{-3}$M	322.6	12.4	57.4	<1	<1

Table 3. Results from x-ray reflectivity and LP-XSW-FY analyses of the partitioning of Pb(II), Cu(II), and Zn(II) between ESHA coatings and α-Al_2O_3(1-102), α-Al_2O_3(0001), and α-Fe_2O_3(0001) surfaces (ESHA concentration = 10g/L, 0.01M $NaNO_3$).

Substrate	Time (hours)	pH	Added [Ca(II)]	Film thickness (Å)	Film-air interface roughness (Å)	Pb% on the surface	Zn% on the surface	Cu% on the surface
The effects of metal-oxide surface								
α-Al_2O_3(0001)	3	6.0±0.05	$2*10^{-3}$M	200.2	8.8	<1	<1	<1
α-Al_2O_3(1-102)	3	6.0±0.05	$2*10^{-3}$M	333.8	16.3	11.4	<1	<1
α-Fe_2O_3(0001)	3	6.0±0.05	$2*10^{-3}$M	349.2	13.4	74.1	3.7	2.4
α-Al_2O_3(0001)	72	6.0±0.05	$2*10^{-3}$M	270.7	18.5	<1	<1	<1
α-Al_2O_3(1-102)	72	6.0±0.05	$2*10^{-3}$M	344.6	23.1	58.3	<1	<1
α-Fe_2O_3(0001)	72	6.0±0.05	$2*10^{-3}$M	542.0	15.2	91.7	7.7	6.4
The effects of pH								
α-Al_2O_3(1-102)	72	9.0±0.1	-	295.3	24.7	54.3	<1	<1
α-Al_2O_3(1-102)	72	6.0±0.05	-	325.8	9.9	39.8	<1	<1
α-Al_2O_3(1-102)	72	4.0±0.05	-	305.3	44.7	3.8	<1	<1

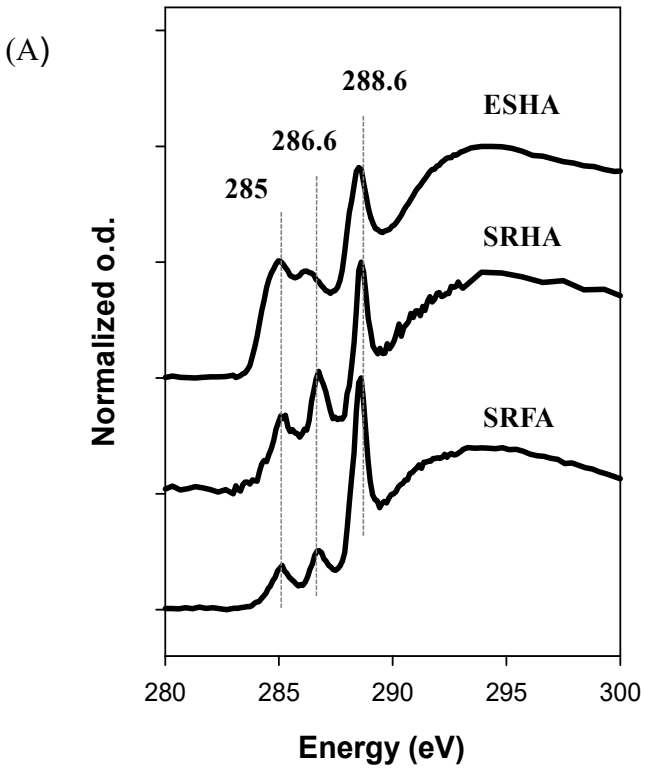

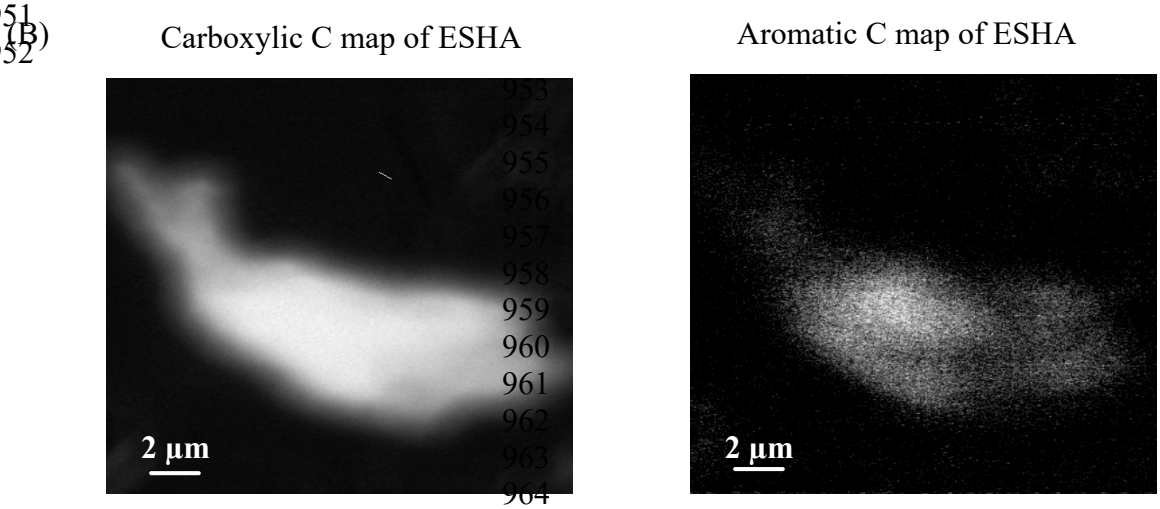

Fig. 1 (A) STXM-based C K-edge NEXAFS spectra for dry humic substances**.** Features marked by dashed lines indicate (i) aromatic (285.0eV), (ii) phenolic (286.6eV), and (iii) carboxylic/peptidic (288.6 eV) functional groups; **(B)** Carboxylic and aromatic C STXM maps of a dry ESHA aggregate.

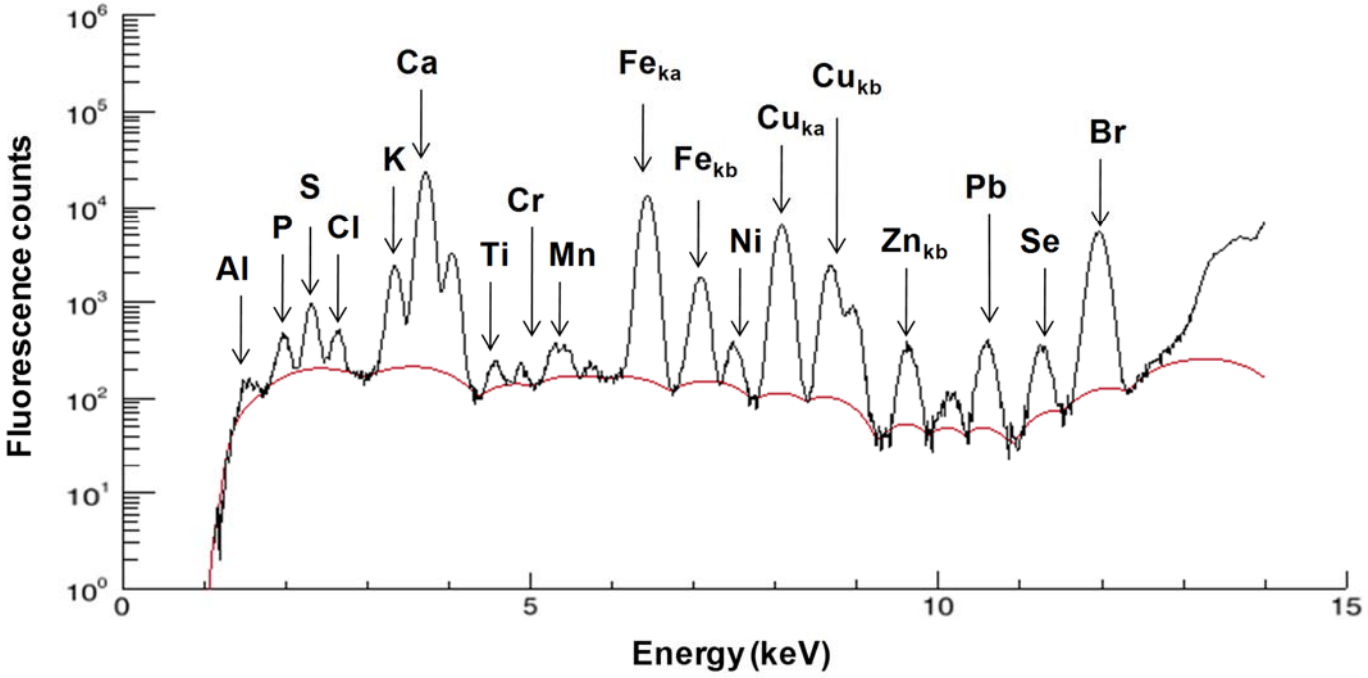

Fig. 2 LP-XSW-FY-generated x-ray fluorescence spectra of the ESHA film (ESHA concentration = 10g/L, 0.01M $NaNO_3$, pH = 6.0, reaction time = 3 hrs, at incidence angle 0.1°).

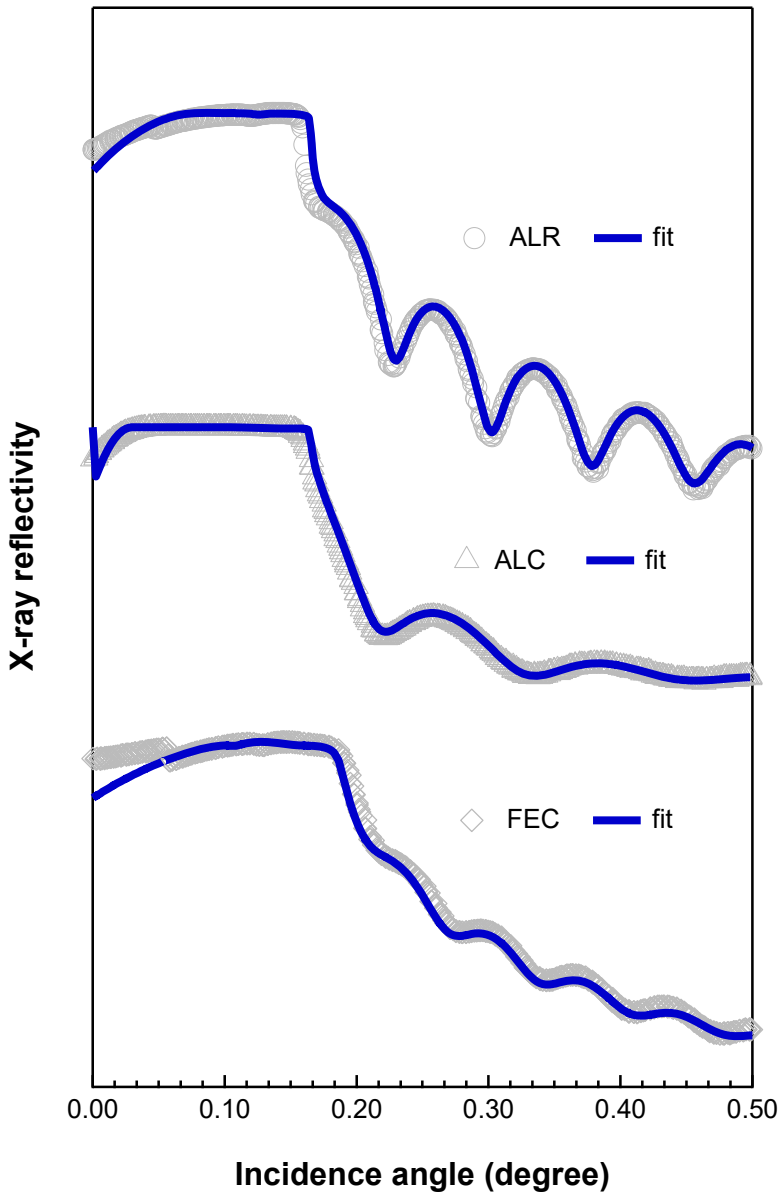

Fig. 3 X-ray reflectivity profiles for ESHA-coated metal-oxide surfaces (ESHA = 10 g/l, 0.01 M $NaNO_3$, pH = 6.0, 2 mM Ca(II), reaction time = 3 hours): ALR is α-Al_2O_3(1-102), ALC is α-Al_2O_3(0001), and FEC is α-Fe_2O_3(0001).

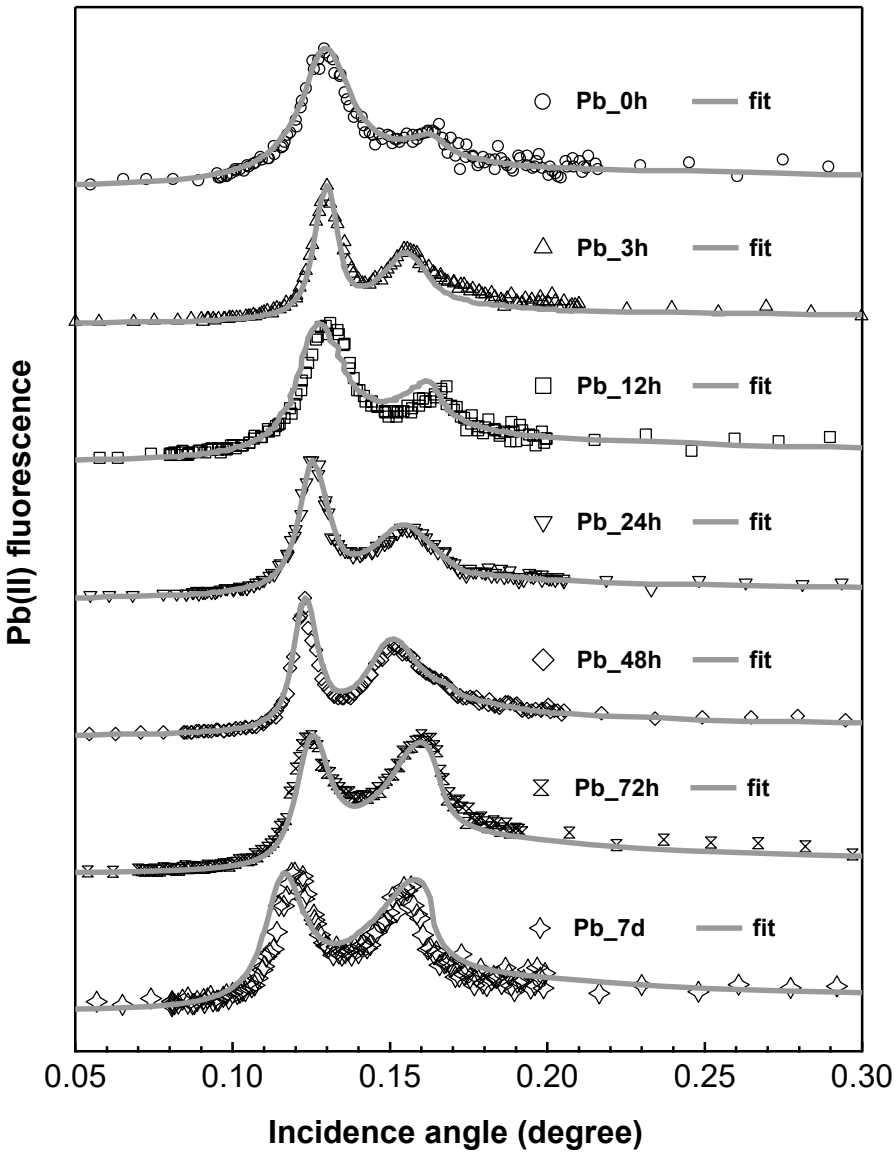

Fig. 4 LP-XSW-FY spectra for Pb(II) distributions at the ESHA-coated α-Al_2O_3 (1-102) surfaces as a function of reaction time (ESHA = 10 g/l, 0.01 M $NaNO_3$, 2 mM Ca(II), pH = 6.0 ± 0.05).

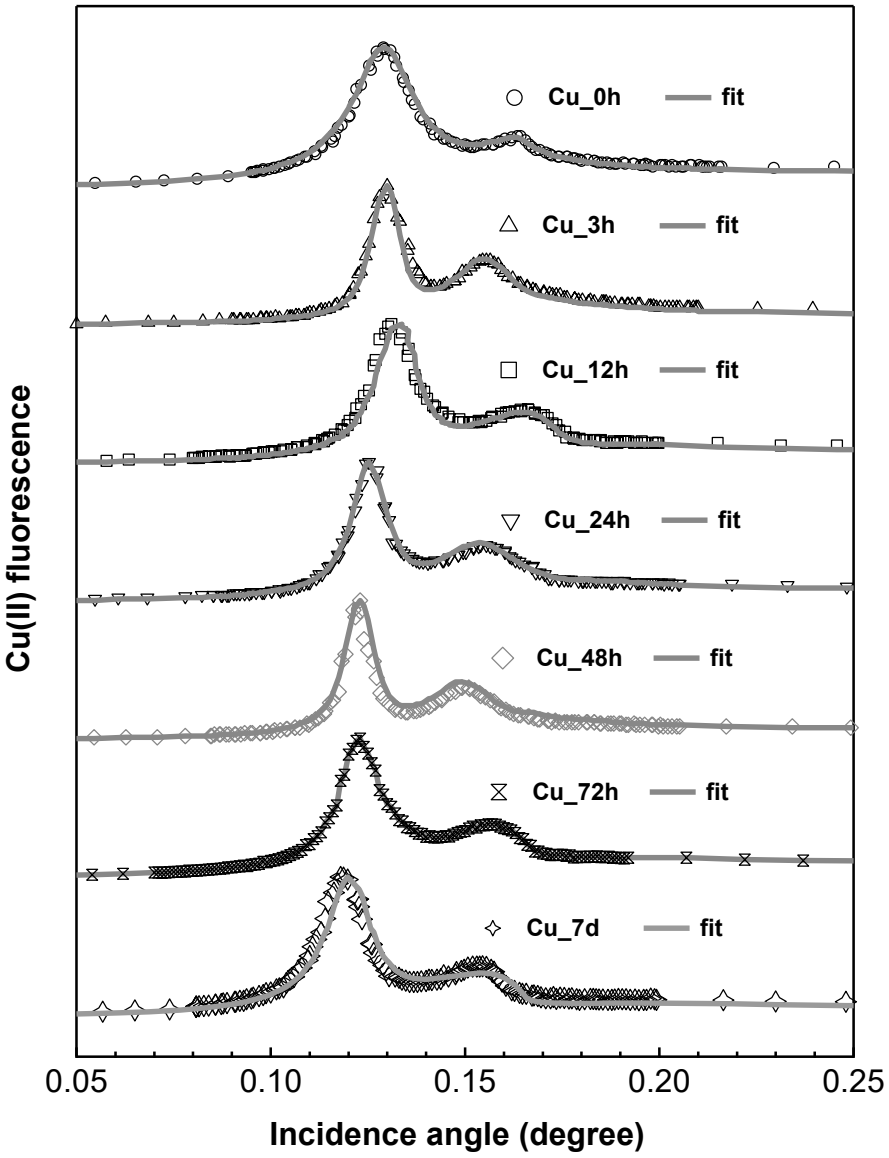

Fig. 5 LP-XSW-FY spectra for Cu(II) distributions at the ESHA-coated α-Al_2O_3 (1-102) surfaces as a function of reaction time (ESHA = 10 g/l, 0.01 M $NaNO_3$, 2 mM Ca(II), pH = 6.0 ± 0.05).

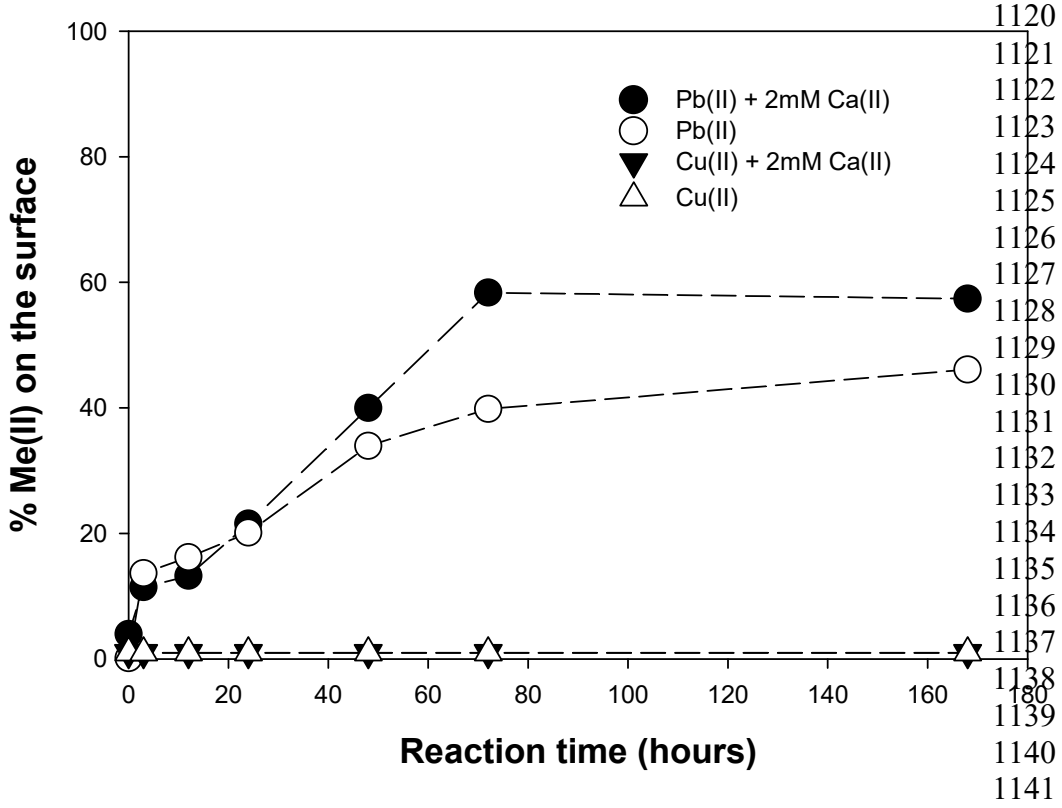

Fig. 6 The effect of calcium on Pb(II) distributions at ESHA-coated α-Al_2O_3 (1-102) surfaces as a function of reaction time.